Accepted: June 05, 2015
1421-9778/15/0366-2121$39.50/0

Original Paper

Sodium Ferulate Prevents Daunorubicin - Induced Apoptosis in H9c2 Cells via Inhibition of the ERKs Pathway

Zhi-Juan Wu Jing Yu Qiu-Juan Fang Rui-Xing Wang Jia-Bian Lian Rui-Lan He Hai-Xia Jiao Mo-Jun Lin

Department of Physiology & Pathophysiology and Laboratory of Cardiovascular Sciences, School of Basic Medical Sciences, Fujian Medical University, Fuzhou, People's Republic of China

Key Words
Sodium Ferulate • Daunorubicin • Cardio-protection • Apoptosis • ERKs • H9c2 cell

Abstract
Background: Daunorubicin (DNR)-induced cardiotoxicity, which is closely associated with cardiomyocyte apoptosis, limits the drug's clinical application. The activation of the extracellular regulated protein kinases (ERKs) pathway is responsible for the pro-apoptosis effect of DNR. Sodium ferulate (SF) has recently been found to attenuate both DNR-induced cardiotoxicity and mitochondrial apoptosis in juvenile rats. Nonetheless, the precise mechanism underlying SF-induced cardio-protection remains unclear. ***Methods:*** The DNR-injured H9c2 cell model was prepared by incubating the cells in 1 μM DNR for 24 h. Amounts of 15.6, 31.3 or 62.5 μM SF were simultaneously added to the cells. The effect of SF on the cytotoxic and apoptotic parameters of the cells was studied by monitoring apoptosis regulation via the ERKs pathway. ***Results:*** SF attenuated DNR-induced cell death (particularly apoptotic death), cTnI and β-tubulin degradation, and cellular morphological changes. SF reduced mitochondrial membrane potential depolarization, cytochrome *c* leakage, and caspase-9 and caspase-3 activation. SF also decreased ERK1/2, phospho-ERK1/2, *p*53 and Bax expression and increased Bcl-2 expression. These effects were similar to the results observed when using the pharmacological ERKs phosphorylation inhibitor, AZD6244. ***Conclusion:*** We determined that SF protects H9c2 cells from DNR-induced apoptosis through a mechanism that involves the interruption of the ERKs signaling pathway.

Introduction

Daunorubicin (DNR), a commonly prescribed anthracycline antibiotic, is an indispensable component of various chemotherapeutic regimens that are used to treat

Z.-J. Wu, J. Yu, Q.-J. Fang and R.-X. Wang have contributed equally to this publication.

Mo-Jun Lin, M.D. Ph.D.
Department of Physiology & Pathophysiology and Laboratory of Cardiovascular Sciences, School of Basic Medical Sciences, Fujian Medical University, 1 Xueyuan Road, Shangjie Zhen, Minhou County, Fuzhou, Fujian Province 350108, (P.R. China)
Tel. 86-591-22862429 (office), 86-13705977819 (mobile), E-Mail mjlin@mail.fjmu.edu.cn

specific types of leukemia (i.e., acute myeloid leukemia and the blastic phase of chronic myelogenous leukemia). However, the clinical application of DNR is seriously limited by its cumulative and dose-dependent cardiotoxicity, which may manifest as potentially fatal dilated cardiomyopathy and congestive heart failure [1, 2]. In spite of the tremendous efforts by clinicians, there are few pharmacological remedies for these cardiotoxic side effects without compromising the antitumor efficacy of DNR [3, 4]. Further research is warranted to seek a novel cardio-protective agent that targets the molecular pathogenesis of DNR-induced cardiotoxicity [5].

DNR-induced cardiotoxicity is thought to be a complex multifactorial process. Increasing amounts of evidence indicate that cardiomyocyte apoptosis may be a prominent contributor to the progression of anthracycline cardiomyopathy [6-8]. However, the signal transduction pathway associated with DNR-induced cardiomyocyte apoptosis and cardiac injury is not completely understood. Recent studies have determined that extracellular regulated protein kinases (ERKs), a subfamily of the mitogen-activated protein kinases (MAPKs), may play an important role in anthracycline-induced cardiotoxicity by exacerbating cardiomyocyte apoptosis and cardiac pathologies [9-11]. Anthracycline induces the activation of ERKs, followed by the activation of the pro-apoptotic proteins *p*53 and Bax and the suppression of the anti-apoptotic protein Bcl-2, a process that ultimately results in cardiomyocyte apoptotic death [11]. Conversely, the inhibition of ERKs may protect against anthracycline cardiotoxicity, as demonstrated previously in multiple *in vivo* and *in vitro* studies [12, 13]. Thus, an ERKs-targeted anti-apoptotic mechanism has been deemed a promising protective strategy against DNR-induced cardiotoxicity.

Sodium ferulate (SF), the sodium salt of ferulic acid (3-methoxy-4-hydroxy-cinamate sodium), is an effective ingredient in Chinese medicinal herbs such as *Angelica sinensis*, *Ferula asafoetida* and *Lignsticum chuangxiong* [14, 15]. It exhibits several pharmacological activities such as anti-oxidative, anti-inflammatory, platelet aggregation inhibitory, antihypertensive and anti-apoptotic effects [16-18]. SF has been approved by the State Drug Administration of China as a treatment for ischemic injury, atherosclerosis and diabetic damage [19-21].

A recent study from our laboratory demonstrated that SF strongly attenuates DNR-induced cardiomyopathy, cardiac dysfunction and mitochondrial myocardial apoptosis in juvenile rats [22]. However, other protective effects of SF, such as the molecular mechanisms underlying its anti-apoptotic effects that protect against DNR-induced cardiotoxicity, remain unknown and warrant further investigation. Increasing amounts of evidence have highlighted the protective effects of SF against cardiomyocyte apoptosis [23, 24]. This anti-apoptotic activity may result from the properties of SF, which is involved in free radical scavenging, the regulation of Ca^{2+} handling, mitochondrial protection and the apoptotic signaling [20, 25-27]. In particular, Ma *et al.* discovered that SF inhibited radiation-induced apoptosis by blunting the activity of ERKs [28, 29]. Based on these findings, we thereby hypothesized that SF may alleviate DNR-induced cardiotoxicity by inhibiting the cardiomyocyte apoptosis mediated by ERKs.

To test this hypothesis, the current study was performed to assess the possible protective and apoptotic inhibitory effects of SF by using a DNR-induced rat cardiomyoblast H9c2 cell model [30]. The effects of SF on mitochondrial dysfunction and the regulation of mitochondrial apoptosis via the ERKs pathway were also explored to uncover the potential mechanisms underlying its anti-apoptotic effect.

Materials and Methods

Reagents

Daunorubicin (DNR) was obtained from Pfizer, Inc. (NY, NY, USA). Sodium ferulate (SF) was kindly provided by Rejuvenation Pharmaceutical Co., Ltd. (Fuzhou, China). All chemicals were reconstituted in sterile saline immediately prior to their use. AZD6244, a mitogen protein kinase (MEK1) inhibitor that also

inhibits ERK1/2 phosphorylation, was purchased from Selleck Chemicals (Houston, TX, USA) and dissolved in DMSO.

Cell culture and viability assay

One rat cardiomyoblast H9c2 cell line and two human carcinoma cell lines (promyelocytic leukemia HL 60 cells and erythromyeloblastoid leukemia K562 cells) were used in this study. The cell lines were purchased from the Cell Bank of the Chinese Academy of Sciences (Shanghai, China); the H9c2 cell line was cultured in Dulbecco's Modified Eagle's Medium (DMEM, GIBCO, Invitrogen, Carlsbad, CA, USA), and the HL 60 and K562 cell lines were cultured in Roswell Park Memorial Institute 1640 medium (RPMI-1640, GIBCO, Invitrogen, Carlsbad, CA, USA). Each cell solution contained 10 % fetal bovine serum (Hyclone, Thermo Fisher Scientific Inc., South Logan, UT, USA), 100 U/mL of penicillin, and 100 μg/mL of streptomycin and was maintained in a humidified incubator at 37 °C with 5 % CO_2.

For the viability assay, the cells were seeded into 96-well culture plates at densities of 2.5×10^4 cells/mL. Twenty-four hours after plating, the cells were treated with 1 μM DNR in either the absence or the presence of varying concentrations of SF for 24 h. Cell viability was assessed by adding 500 μg/mL of MTT reagent (3-(4,5-dimethylthiazol-2-yl)-2,5-diphenyltetrazolium bromide, Sigma-Aldrich, St Louis, MO, USA) to the medium for 4 h. The supernatant was removed carefully, and 200 μL of DMSO was added to each well to dissolve the insoluble formazan product into a colored solution. The absorbance was measured at 570 nm in a microplate reader (Elx800, BioTek, Winooski, VT, USA). The following equation was used to measure cell viability: cell viability=OD treatment group/OD control group×100 %. The IC_{50} values were determined from the dose-response plots by linear regression. Each of the experiments was performed at least three times.

Annexin V/PI double-staining assay

An FITC Apoptosis Detection Kit (BD Pharmingen, San Jose, CA, USA) was utilized to determine the numbers of apoptotic cells. The cells were collected, washed and then re-suspended in 1× binding buffer containing 5 μL of FITC annexin V and 5 μL of propidium iodide (PI). Following a short incubation period of 15 min in the dark at room temperature, the fluorescence of the cells was immediately analyzed using FACSVerse flow cytometry (BD Biosciences, San Jose, CA, USA). The fluorescence emission signals for FITC annexin V were plotted against PI to distinguish among viable cells (i.e., annexin V and PI negative), early apoptotic cells (annexin V positive and PI negative) and late apoptotic or necrotic cells (both annexin V and PI positive). An analysis was performed using the FlowJo 7.6 analysis software (Treestar Inc., Ashland, OR, USA). Each measurement was performed in triplicate.

Mitochondrial membrane potential assay

Mitochondrial membrane potential (ΔΨm) was monitored using the mitochondrial sensitive probe rhodamine 123 (Sigma-Aldrich, St Louis, MO, USA), which accumulated in the mitochondrial matrix in a manner dependent on the organelle's electrochemical gradient. The depolarization of ΔΨm results in the loss of rhodamine 123 from the mitochondria and in a corresponding decrease in intracellular green fluorescence. Following the indicated treatments, the H9c2 cells were incubated with 10 μg/mL rhodamine 123 for 20 min, followed by three washes with cold PBS to remove the extracellular rhodamine 123. Data acquisition and analysis were executed using FACSVerse flow cytometry (excitation and emission wavelengths of 488 and 525 nm, respectively). Fluorescence intensity was quantified based on the positive rate of rhodamine 123. Changes in rhodamine 123 fluorescence were calculated using an index of variation (IV), as determined by the following formula: IV= (MT – MC)/MC, where MT is the median of fluorescence for the treated samples, and MC is the median for the control samples [31]. Negative IV values paralleled the depolarization of the mitochondrial membrane. All experiments were repeated at least three times; representative data are presented in the appropriate figures and tables.

Western blot analysis

The cells were collected and lysed in 0.1 mL of ice-cold RIPA lysis buffer (Beyotime Biotechnology, Shanghai, China) on ice for 30 min. The total protein concentration was measured using a bicinchoninic acid assay (Beyotime Biotechnology, Shanghai, China). The protein samples (30 μg) were subjected to 10

% SDS-PAGE and transferred electrophoretically onto polyvinylidene difluoride (PVDF) membranes. The membrane was blocked with a blocking solution (5 % (wt/vol) nonfat dry milk in Tris buffered saline with Tween 20) for 1 h at room temperature. The membrane was then incubated at 4 °C overnight with anti-cTnI (1:1000 dilution, Santa Cruz, Dallas, TX, USA), β-Tubulin (1:1000 dilution, Cell Signaling Technology, Danvers, MA, USA), cytochrome *c* (1:1000 dilution, Santa Cruz, Dallas, TX, USA), ERK1/2 (1:1000 dilution, Santa Cruz, Dallas, TX, USA), P-ERK1/2 (1:500 dilution, Santa Cruz, Dallas, TX, USA), *p*53 (1:1000 dilution, Santa Cruz, Dallas, TX, USA), Bax (1:500 dilution, Santa Cruz, Dallas, TX, USA), Bcl-2 (1:500 dilution, Santa Cruz, Dallas, TX, USA), GAPDH (1:1000 dilution, Cell Signaling Technology, Danvers, MA, USA) and VDAC1 (1:1000 dilution, Cell Signaling Technology, Danvers, MA, USA) primary antibodies. The membrane was then washed and probed with horseradish peroxidase-conjugated secondary antibody (1:2000 dilution, Cell Signaling Technology, Danvers, MA, USA). The immunoreactive proteins were visualized using a BeyoECL Plus Kit (Beyotime biotechnology, Shanghai, China). Protein bands were quantified via densitometry using Quantity One software (Bio-Rad, Hercules, CA, USA).

Mitochondrial cytochrome c, Bax and Bcl-2 assay

Mitochondrial extracts were prepared using the Cell Mitochondria Isolation Kit (Beyotime Biotechnology, Shanghai, China) according to manufacturer's instructions. Purity of the mitochondrial fraction was assessed by VDAC1 (a mitochondrial marker) and GAPDH (a cytosolic marker). The levels of cytochrome *c*, Bax, and Bcl-2 in mitochondrial protein were subsequently immunodetected via Western blot analysis.

Enzymatic assay for caspase-3 and caspase-9 activity

Caspase activity was detected using the caspase-3 and caspase-9 Colorimetric Assay Kit (KeyGen Biotech CO., Ltd., Nanjing, China) and standard procedures. The cells (3×10^6) were collected and then resuspended in lysis buffer. The supernatants were subsequently extracted, and the protein concentrations were measured using the BCA method. An equal amount (100 μg) of protein was diluted to 50 μL lysis buffer for each assay. The reaction mixture contained 50 μL of 2× reaction buffer, 50 μL of cell lysates and 5 μL of chromogenic substrates. The reaction was carried out at 37 °C for 4 h; the absorbance in the wells was measured at 405 nm by a microtiter plate reader. The fold increases in the enzymatic activity of both caspase-3 and caspase-9 were determined by comparing these results with the level of the un-induced control.

Statistical analysis

Data are presented as the means ± S.E. Statistical significance was evaluated using Student's t-tests and ANOVA where appropriate. Statistical significance was defined as $P<0.05$. The calculations were performed using SPSS 11.0 statistical software (SPSS Inc., Chicago, IL, USA). Curve fitting was performed using SigmaPlot 11.0 software (Systat Software Inc., Chicago, IL, USA).

Results

SF depressed DNR-induced cell death in H9c2 cells

We treated the H9c2 cells with SF (15.6, 31.3 and 62.5 μM) in the absence of daunorubicin for 24 h. As shown in Fig. 1A, SF alone did not cause any statistically significant changes in cell viability, which indicated that SF itself did not exert any cytotoxic effects on the H9c2 cells.

Cell viability was subsequently examined following the incubation of the combination of SF and DNR to analyze the protective effects exerted by SF against DNR-induced cytotoxicity. DNR treatment triggered H9c2 cell death. As shown in Fig. 1B, cell viability decreased to 70.9±2.6 % following exposure to 1 μM DNR for 24 h. SF attenuated DNR-induced growth inhibition. The viabilities increased by 15.59 %, 83.96 %, and 78.40 % for the SF concentrations of 15.6, 31.3 and 62.5 μM, respectively. Significant differences were noted at doses of 31.3 and 62.5 μM (cell viability: 95.3±1.8 % and 93.7±2.2 %, respectively) compared to treatment with DNR alone ($P<0.05$, n=3). No significant difference in the dose-response was noted between the concentrations of 15.6 μM and 62.5 μM.

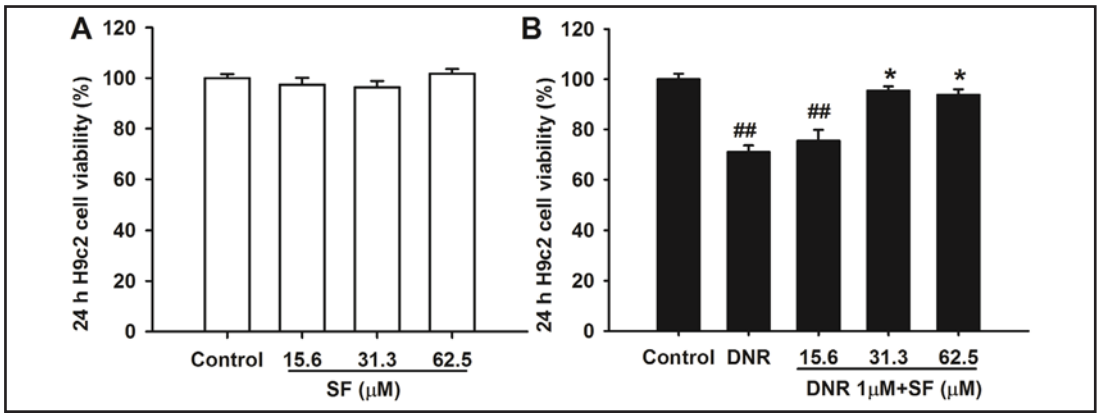

Fig. 1. The effects of SF on DNR-induced H9c2 cell death. The viability of H9c2 cells exposed to SF in either the absence (A) or the presence (B) of DNR in *vitro* for 24 h. Data are expressed as the means ± S.E and represent three independent experiments. ## P<0.01 vs. Control, * P<0.05 vs. DNR.

SF did not undermine the antineoplastic effect of DNR in either the HL 60 cells or the K562 cells

DNR is most commonly used to treat specific types of leukemia, including acute myelogenous leukemia and the blastic phase of chronic myelogenous leukemia. Thus, HL 60 and K562 cell lines were used to exclude the possible interference of SF with DNR's antineoplastic effects in the setting of cancer therapy.

For these two cell lines, the viabilities of SF and DNR co-treated cells were 16.30±1.15 % and 53.0±1.12 %, 14.44±0.87 %, and 55.72±0.93 %, and 15.05±0.63 % and 54.35±1.67 % at the concentrations of 15.6 μM, 31.3 μM, and 62.5 μM SF, respectively (Fig. 2). As shown in Fig. 2, no significant difference was observed among these results compared with DNR treatment alone.

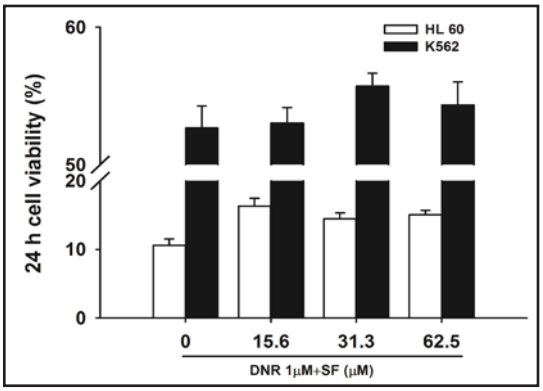

Fig. 2. The effect of SF on DNR's antineoplastic activity. HL60 and K562 cell viability following co-treatment with SF and DNR for 24 h. Data are expressed as the means ± S.E and represent three independent experiments.

Table 1. IC_{50} values of the growth inhibition of HL 60 and K562 cell lines by DNR in the absence and presence of 15.6, 31.3 or 62.5 μM of SF. Data are expressed as the means ± S.E and represent three independent experiments

	HL 60 (nM)	K562 (nM)
DNR	328.6±18.6	512.7±21.5
DNR + 15.6 μM SF	341.7±12.4	503.6±19.8
DNR + 31.3 μM SF	321.4±23.2	537.3±17.2
DNR + 62.5 μM SF	334.8±19.1	494.8±23.5

The IC_{50} values of the growth inhibition of the HL 60 and K562 cell lines by DNR in the absence and presence of 15.6, 31.3, or 62.5 μM of SF were subsequently determined. After incubation for 24 h, DNR had significant and dose-dependent anti-proliferative effects on both cell lines. The IC_{50} values were 328.6±18.6 and 512.7±21.5 nM in HL 60 and K562 cells, respectively (Table 1). The presence of 15.6, 31.3 and 62.5 μM SF had little or no effect on the IC50 value for DNR in HL 60 and K562 cells (P>0.05, Table 1). Our data indicated that SF did not decrease the antineoplastic activity of DNR in these two carcinoma cell lines.

SF reversed DNR-induced morphological changes

Cell morphology was examined using Wright's Giemsa staining. As shown in Fig. 3A, untreated H9c2 myoblasts were spindle-to-stellate-shaped cells with integral and clear

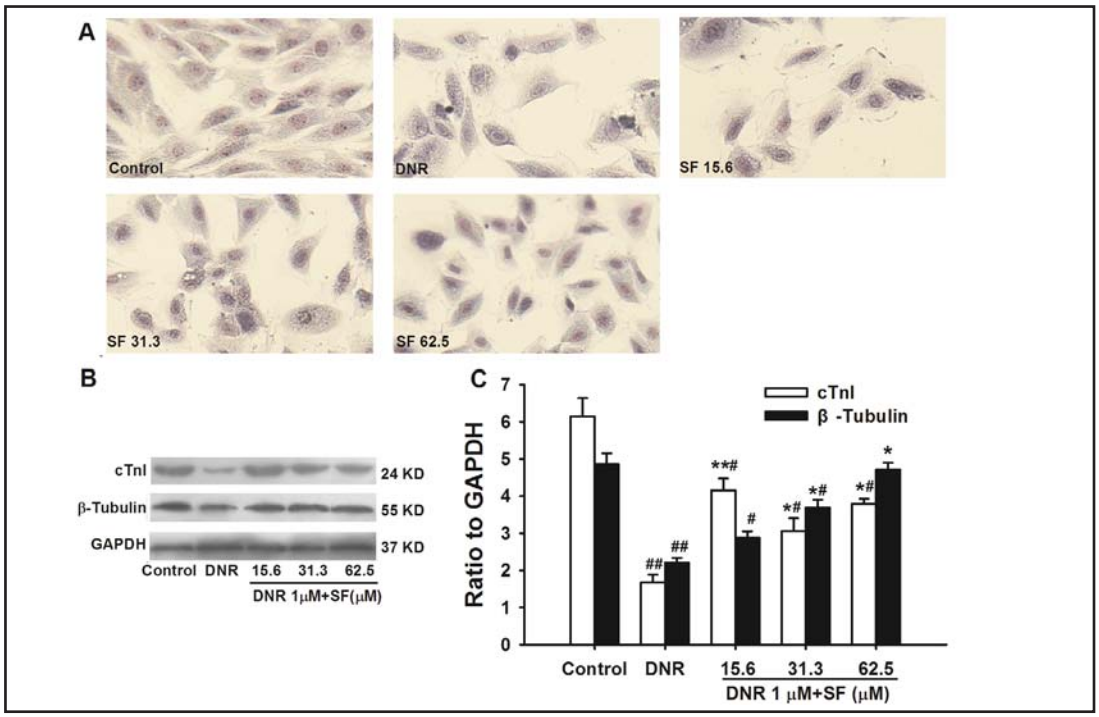

Fig. 3. The effect of SF on DNR-induced cellular injury in H9c2 cells. H9c2 cells were treated with 1 μM DNR and co-treated with different concentrations of SF (15.6, 31.3 and 62.5 μM) for 24 h. A: The morphology of H9c2 cells treated with DNR and SF. Representative images of Wright's Giemsa staining are presented. Magnification×400. B: A representative image of cTnI and β-Tubulin protein expression as determined by Western blotting. C: The results of an optical density analysis of protein bands. Data are expressed as the means ± S.E and represent three independent experiments. # P< 0.01, ## P< 0.01 *vs.* Control; * P< 0.05, ** P< 0.01 *vs*. DNR.

structures. Their incubation with DNR caused alterations in cell shape, including cell shrinkage, cell rounding and membrane blebbing, as well as the development of multiple constrictions. The apoptotic cells, which exhibited deep blue karyotin staining, chromatin margination, apoptotic bodies, and karyopyknosis, were also observed. In contrast, co-treatment with SF produced a reversal of the DNR-induced morphological changes, particularly following the 31.3 and 62.5 μM SF incubations, as the cells appeared to recover their normal shapes.

SF mitigated the cTnI and β-Tubulin degradation caused by DNR

cTnI and β-Tubulin are key components of myofilaments and microtubules, respectively. The release of cardiac troponin (cTnI) is a sensitive and specific marker of myocardial injury and is associated with contractile dysfunction [32-34]. β-Tubulin degradation contributes to the development of cardiac arrhythmia, Ca^{2+} handling disorders and stress-strain effects in anthracycline-injured hearts [35].

In this study, DNR-induced cell injury was accompanied by the degradation of cTnI and β-Tubulin (P<0.01, Fig. 3B and 3C). A combination of different concentrations of SF and 1 μM DNR prevented the degradation of both cTnI and β-Tubulin (P<0.05, vs. DNR).

SF attenuated DNR-mediated cellular damage via apoptosis inhibition

By measuring apoptotic cell death (i.e., early and late apoptosis) via the FACS-based quantization of annexin V-positive cells, we observed that DNR largely promoted apoptotic cell death. The percentage of cells labeled with annexin V (+) PI (-) and annexin V (+) PI (+) increased from 3.13±0.41 % to 21.63±2.90 % (P<0.01, DNR *vs.* Control) (Fig. 4A and 4B).

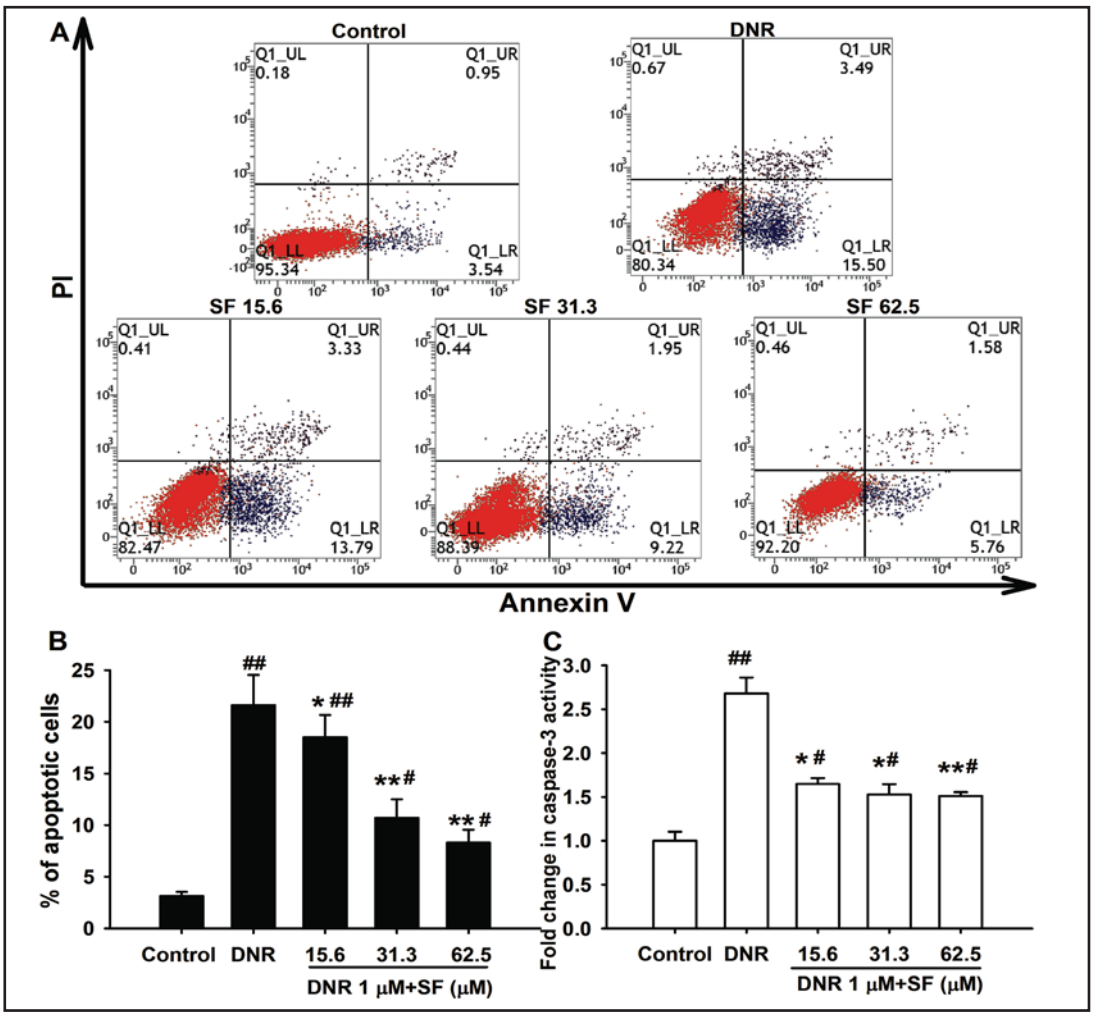

Fig. 4. The effect of SF on apoptosis induced by DNR in H9c2 cells. A: A scatterplot depicting the distribution of cells stained with annexin V along the x-axis and cells stained with propidium iodide (PI) along the y-axis. A representative result was presented. B: The combined results of three separate FACS analyses depicting the mean levels of apoptotic cells (annexin V^+ PI^- &. annexin V^+ PI^+). Caspase-3 activity (C) induced by DNR in H9c2 cells. Data are expressed as the means ± S.E and represent three independent experiments, # P<0.05, ## P<0.01 vs. Control; * P<0.05, ** P<0.01 vs. DNR.

In line with the annexin V/PI staining results, the enzymatic activity of caspase-3, a marker of apoptosis, was also found to be significantly increased in DNR-treated cells (Fig. 4C). SF clearly blocked this pro-apoptotic effect. As depicted in Fig. 4A and 4B, the percentages of apoptotic cells decreased to 18.51±2.16 %, 10.69±1.81 % and 8.31±1.23 % for the SF concentrations of 15.6, 31.3 and 62.5 μM, respectively. Further, the enzymatic activity of caspase-3 also decreased by 38.51 %, 42.95 %, and 43.62 %, respectively.

SF limited the pro-apoptotic effects of DNR on mitochondrial membrane potential collapse, mitochondrial cytochrome c release, and caspase-9 activation

Mitochondrial membrane potential collapse, cytochrome *c* release and subsequent caspase-9 and caspase-3 activation lead to apoptosis. This cascade has been proven to be the primary apoptotic pathway in anthracycline-treated H9c2 cells [36]. Consistent with previous reports, the exposure of H9c2 cells to DNR (1 μM) for 24 h resulted in the same types of events, as follows: the dissipation of Rhodamine 123 fluorescence (IV=−0.34), the reduction of mitochondrial cytochrome *c* content, and the amplification of caspase-9 enzymatic

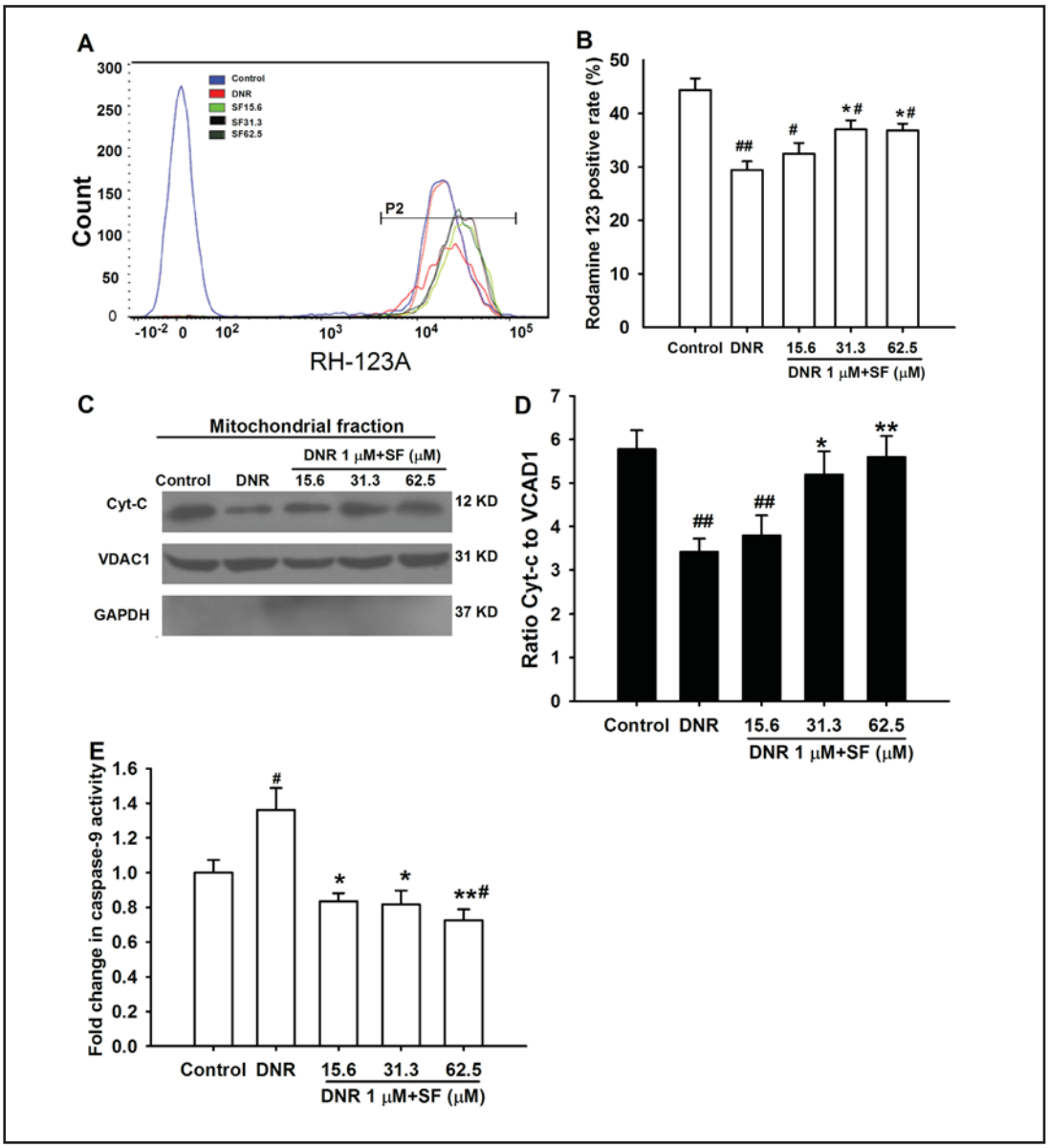

Fig. 5. The effect of SF on mitochondrial membrane potential, cytochrome *c* (Cyt-c) release, caspase-9 gene expression and enzymatic activity. A: Mitochondrial membrane potential was examined via flow cytometry with a rhodamine 123 probe treatment. Data from one representative experiment are presented. B: The combined results of three separate FACS analyses depicting the intensity of rhodamine 123 florescence. C: A representative image of Cyt-*c* protein expression in mitochondrial fractions as determined by Western blotting. Mitochondrial Marker VDAC1 immunoblot was used as a control for equal loading. D: The quantification of mitochondrial cytochrome *c*. Caspase-9 activity (E) induced by DNR in H9c2 cells. Data are expressed as the means ± S.E and represent three independent experiments, # $P<0.05$, ## $P<0.01$ vs. Control; * $P<0.05$, ** $P<0.01$ vs. DNR.

activity ($P<0.01$ vs. Control) (Fig. 5). Conversely, adjunct treatment with SF facilitated the gradual recovery of mitochondrial membrane potential, as demonstrated by the increased rhodamine 123 fluorescence intensity, with IV values of -0.27, -0.17 and -0.17 (Fig. 5A and 5B). Meanwhile, the mitochondrial proportions of cytochrome *c* increased by 11.11 %, 52.20 and 63.93 % compared with DNR (Fig. 5C and Fig. 5D). SF also decreased the expression of caspase-9 enzymatic activity (Fig. 5E). The changes were statistically significant at the three concentrations indicated previously ($P<0.05$, *vs.* DNR). These results suggested that

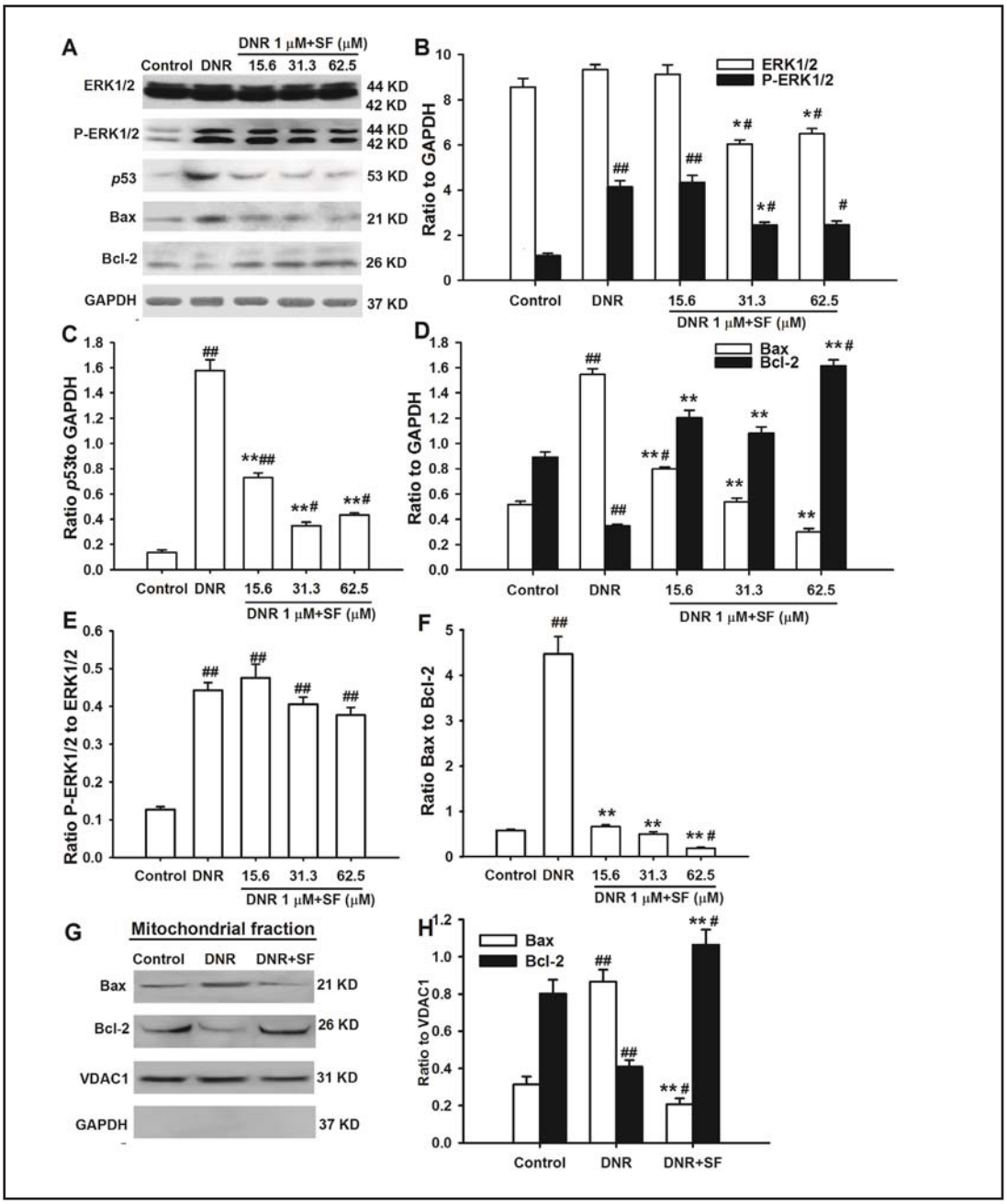

Fig. 6. The effects of SF on the expression patterns of apoptosis regulatory proteins induced by DNR in H9c2 cells. A: Representative ERK1/2, P-ERK1/2, *p*53, Bax and Bcl-2 immunoblots of the whole cell lysate. Equal protein loading was confirmed by GAPDH levels. A quantitative analysis of the ratios of ERK1/2 and P-ERK1/2 (B), *p*53 (C) and Bax and Bcl-2 (D) to GAPDH. A quantitative analysis of the ratios of P-ERK to ERK1/2 (E) and Bax to Bcl-2 (F). G: Redistribution of Bax and Bcl-2 in mitochondria. Cells were treated with 1 μM DNR in the absence and presence of 62.5 μM of SF for 24 h. Subcellular fractions of mitochondria were prepared and subjected to Western blot analysis. Mitochondrial Marker VDAC1 immunoblot was used as a control for equal loading. H: Mean intensity of mitochondrial Bax and Bcl-2 determined by densitometric analysis. Data are expressed as the means ± S.E and represent three independent experiments, # $P<0.05$, ## $P<0.01$ vs. Control; * $P<0.05$, ** $P<0.01$ vs. DNR.

the SF-mediated cardio-protection observed during DNR treatment is associated with the preservation of mitochondrial function.

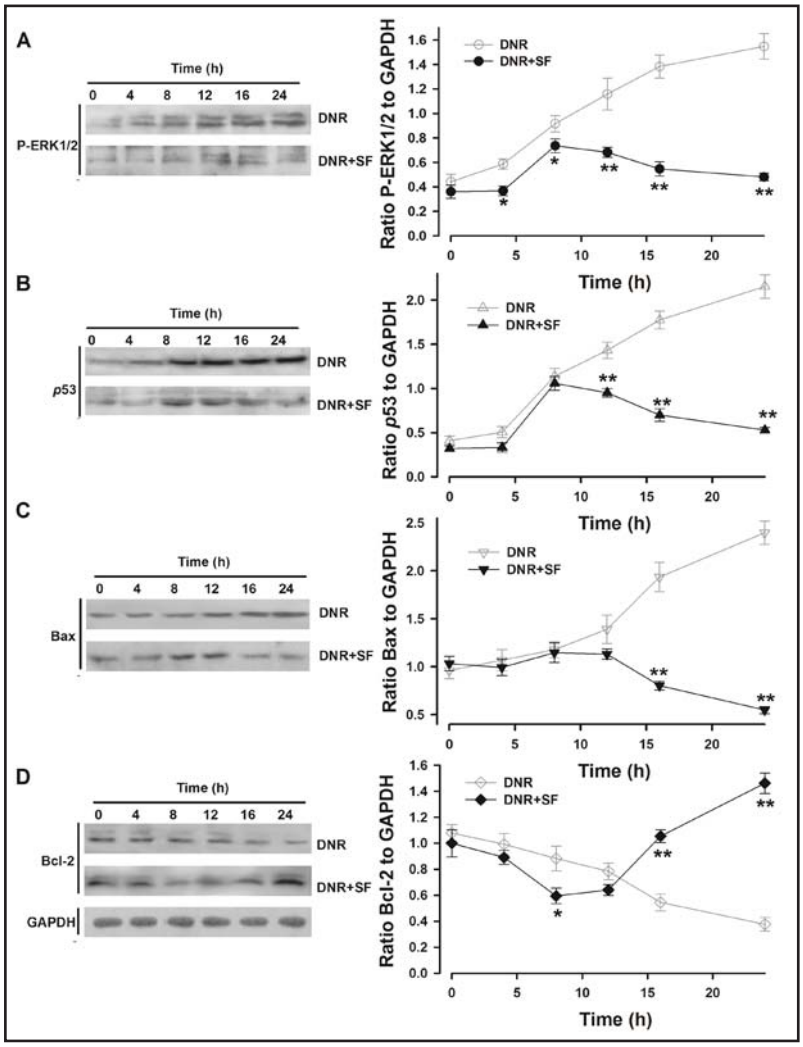

Fig. 7. The effects of SF on the expression of P-ERK1/2 (A), *p*53 (B), Bax (C), and Bcl-2 (D) during the time course. The H9c2 cells were treated with 1 μM DNR in the absence and presence of 62.5 μM of SF for 24 h. Representative Western blots are shown at *left*. The results of an optical density analysis of protein bands are shown at *right*. Data are expressed as the means ± S.E and represent three independent experiments, * $P<0.05$, ** $P<0.01$, DNR vs. DNR+SF.

SF exerted a regulatory effect on the expression of ERK1/2, phospho-ERK1/2, p53, Bax and Bcl-2 in DNR-treated H9c2 cells

We demonstrated that SF markedly reduced DNR-induced cardiotoxicity, a phenomenon that was largely dependent on SF's ability to inhibit apoptosis. DNR causes the activation of extracellular signal-regulated kinases (ERKs), which reportedly triggers a mitochondrial apoptotic pathway. Accordingly, we investigated the mechanism underlying the protective effect of SF against DNR-induced myocardial apoptosis, with an emphasis on the ERKs signaling pathway.

With this aim, the expression levels of the apoptosis-related proteins ERK1/2, phospho-ERK1/2, *p*53, Bax, and Bcl-2 were examined. In these experiments, DNR induced apoptosis, which was accompanied by conspicuous increases in phosphorylated ERK1/2, *p*53, and Bax protein content and by decreases in the expression of Bcl-2 (Fig. 6A-D). The active proportion of ERKs (Ratio of P-ERK1/2 to ERK1/2) was increased by 248 % ($P<0.01$, Fig. 6E). We further detected Bax and Bcl-2 expression in mitochondria by immunoblotting. As shown in Fig. 6G and 6H, DNR enhanced Bax accumulation in mitochondria but depressed the proportion of mitochondrial Bcl-2 ($P<0.01$), which suggested the translocation of Bax and Bcl-2 in mitochondria and the activation of pro-apoptotic Bax.

SF co-treatment neutralized the DNR-mediated disorder noted in the mentioned apoptosis regulatory proteins. As illustrated in Fig. 6A and 6B, SF inhibited the phosphorylation of ERK1/2, which was accompanied by a decreased total ERK1/2 expression level. The middle and high doses of SF (31.3 μM and 62.5 μM) each exerted a marked effect ($P<0.05$, vs.

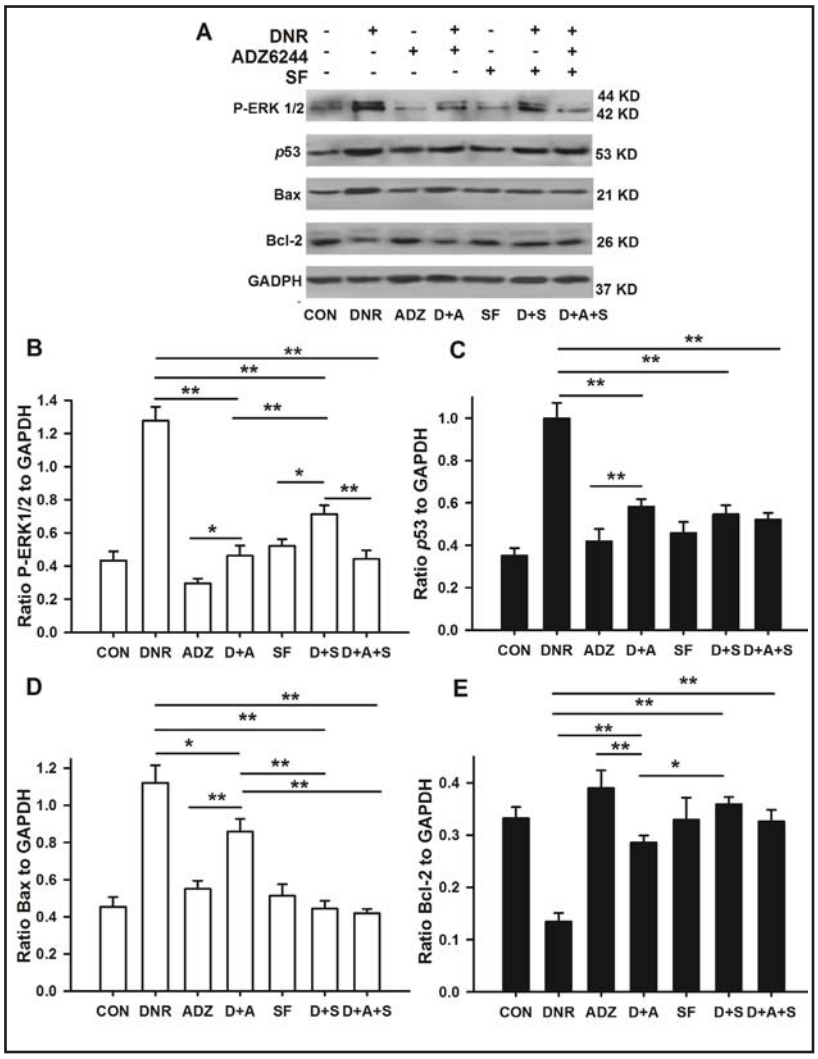

Fig. 8. The effects of ADZ6244 on the expression patterns of apoptosis regulatory proteins induced by DNR. The H9c2 cells were treated with vehicle (CON), 1 μM DNR (DNR), 1 μM ADZ6244 (ADZ), 62.5 μM SF (SF) or a combination of 1 μM DNR and 62.5 μM SF (D+S) for 24 h, with ADZ6244 pre-incubation for 1 h followed by DNR (D+A) or DNR and SF co-incubation (D+A+S) for 24 h. A: A representative image of a Western blot. A quantitative analysis of the ratios of P-ERK1/2 (B), *p*53 (C), Bax (C) and Bcl-2 (D) to GAPDH. Data are expressed as the means ± S.E and represent 3 independent experiments, * $P<0.05$, ** $P<0.01$.

DNR). Similarly, SF incubation suppressed the expression of both *p*53 and Bax but prevented a decrease in the expression of the Bcl-2 protein ($P<0.01$, vs. DNR) (Fig. 6A, 6C, and 6D). By statistically calculating the Bax to Bcl-2 ratio with respect to the protein levels, SF was shown to facilitate a recovery from the DNR-induced decreases in the protein expression of the Bax/Bcl-2 ratio (Fig. 6F). Consistent with the results obtained for the whole cell lysate, the DNR-mediated redistribution of Bax and Bcl-2 in mitochondria was effectively blocked by SF co-treatment (Fig. 6G and 6H).

Moreover, by monitoring these proteins during a time course, we observed that DNR produced a time-dependent activation of ERK1/2, *p*53 and disturbed the expression of Bax, Bcl-2 (Fig. 7). The effects of DNR on these proteins were blunted by SF. Compared with DNR alone treatment, the suppression of both phospho-ERK1/2 and downstream *p*53, respectively, began at 4 h and 12 h of SF incubation (Fig. 7A and 7B), whereas the restoration of Bax and Bcl-2 began at 16 h of SF incubation (Fig. 7C and 7D). SF-induced ERK1/2 inhibition was a pioneer in these subsequent events.

The effects of AZD6244 on DNR-treated H9c2 cells

To determine whether the inhibition of extracellular signal-regulated kinase (ERK) is involved in the protective effect exerted by SF, H9c2 cells were pretreated with 1 μM AZD6244, a selective inhibitor of ERK1/2 phosphorylation, for 60 min before being exposed to 1 μM DNR for 24 h.

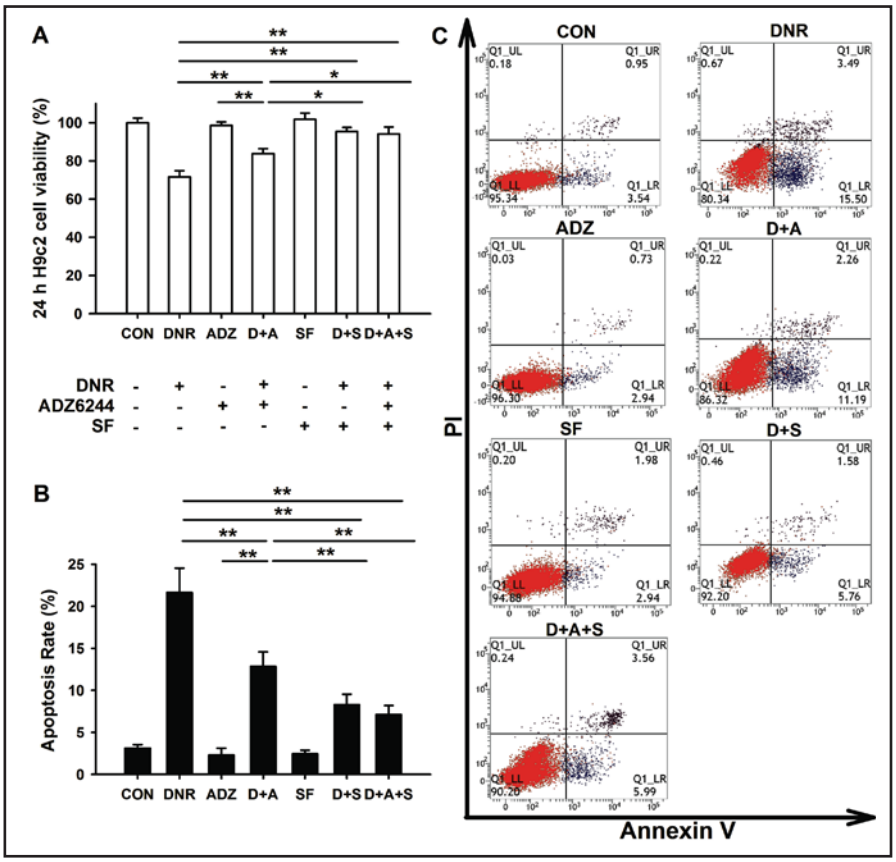

Fig. 9. The effects of ADZ6244 on both cell viability and apoptosis. The H9c2 cells were treated with vehicle (CON), 1 μM DNR (DNR), 1 μM ADZ6244 (ADZ), 62.5 μM SF (SF) or a combination of 1 μM DNR and 62.5 μM SF (D+S) for 24 h, with ADZ6244 pre-incubation for 1 h followed by DNR (D+A) or DNR and SF co-incubation (D+A+S) for 24 h. A: A cell viability assay. B: The combined results of three separate FACS analyses depicting the mean levels of the apoptotic cells (annexin V+ PI− &. annexin V+ PI+). C: A scatterplot depicting the distribution of the cells stained with annexin V along the x-axis and the cells stained with propidium iodide (PI) along the y-axis. A representative result is presented. Data are expressed as the means ± S.E and represent three independent experiments, * P<0.05, ** P<0.01.

As shown in Fig. 8A and 8B, AZD6244 pre-incubation effectively decreased DNR-induced ERKs phosphorylation by 68.58 % (DNR+AZD6244 *vs.* DNR, $P<0.01$). In the presence of AZD6244, DNR-induced growth inhibition was compromised, as evidenced by decreased apoptotic cell numbers and improved cell viability ($P<0.01$, Fig. 9). Following ERKs inactivation, both *p*53 and Bax overexpression and Bcl-2 degradation were prevented by AZD6244 pre-exposure (Fig. 8 C-E). These findings were similar to the results observed when SF was co-incubated with DNR. When AZD6244 was combined with SF, cell viability increased to 94.13±3.62 %, and the apoptosis rate decreased to 7.13±1.06 % (DNR+AZD6244+SF *vs.* DNR, $P<0.01$, Fig. 9). Based on the results of our statistical analysis, the combined use of AZD6244 and SF exerted a stronger protective effect than did AZD6244 treatment alone (DNR+AZD6244+SF *vs.* DNR+AZD6244, $P<0.05$), but no statistically significant difference was noted when these results were compared with the results of SF treatment alone in DNR-damaged H9c2 cells (DNR+AZD6244+SF *vs.* DNR+SF, $P>0.05$, Fig. 9). Additionally, both AZD6244 alone and AZD6244 in combination with SF were more effective than SF treatment alone in diminishing DNR-induced ERKs over-activation, as evidenced by a lower phospho-ERK1/2 level (DNR+AZD6244+SF or DNR+AZD6244 *vs*. DNR+SF, $P<0.05$) but equally suppressed *p*53 ($P>0.05$, Fig. 8A-C). It is noteworthy that SF was more effective at restoring Bax and Bcl-2 (DNR+AZD6244+SF or DNR+SF *vs*. DNR+AZD6244, $P<0.05$) (Fig. 8D and 8E), which was consistent with the lower apoptosis rate noted in the presence of SF. Collectively, all of these data indicated that the inhibition of the ERKs signaling pathway is one of the cardio-protective and anti-apoptotic mechanisms facilitated by SF. However, additional mechanisms may also exist.

Discussion

In the current study, we attempted to assess the protective effect of SF against DNR-induced cardiotoxicity and cardiomyocyte apoptosis using an in *vitro* model of an H9c2 cell line. The results of our study indicated that SF co-treatment effectively attenuated DNR-induced cytotoxicity (particularly apoptotic death) and reduced cTnI and β-Tubulin degradation and morphological changes in DNR-damaged H9c2 cells. At doses that elicited protection, the combination of SF and DNR did not diminish DNR's antineoplastic activity. SF curbed the DNR-induced mitochondrial membrane potential collapse, cytochrome *c* release and caspase-9 and caspase-3 activation, which implied that the mitochondrial apoptotic pathway was inhibited. These changes were associated with the inhibition of the ERKs signaling pathway. SF quelled the over-activation of both ERK1/2 and *p*53 and facilitated the up-regulation of Bcl-2 and the down-regulation of Bax, which enhanced the cellular anti-apoptotic effects indicated above. Therefore, we illustrated that SF protected H9c2 cells from DNR-induced mitochondrial apoptosis via a mechanism that entails the interruption of the ERKs signaling pathway.

Anthracyclines predispose cardiomyocytes to apoptotic death. Excessive apoptosis destroys myocytes and eventually leads to the development of cardiac dysfunction and heart failure [7]. Consistent with the results of our recent report, this paper further demonstrated SF's anti-apoptotic efficacy [37]. We found that DNR treatment incited apoptosis in H9c2 cells, as demonstrated by the dramatically improved positive percentages of annexin V staining and caspase-3 enzymatic activity levels noted during this study. Remarkably, SF counteracted the pro-apoptotic effects of DNR and may therefore protect against DNR-induced cardiotoxicity. In response to SF co-treatment, the percentages of apoptotic cells decreased by 14.42 %, 50.58 %, and 61.58 %, respectively. These results were further demonstrated by the decreased enzymatic activity of caspase-3, which acts as an essential executor and biomarker of apoptosis in mammalian cells.

The mitochondrial apoptotic pathway is more active in anthracycline-injured H9c2 myoblasts and therefore contributes to anthracycline-induced toxicity in immature hearts [36]. Cardiac mitochondria are established key mediators of anthracycline-induced cardiomyocyte apoptosis [6, 38]. DNR accumulates and generates ROS in mitochondria, causing mitochondrial damage and dysfunction [38, 39]. Mitochondrial damage may trigger cardiomyocyte death by activating the mitochondrial intrinsic apoptotic pathway, which leads to mitochondrial permeability transition (MPT), mitochondrial membrane potential dissipation ($\Delta\Psi_m$) and cytochrome *c* release. Following its release from mitochondria, cytochrome *c* activates both caspase-9 and caspase-3, which ultimately initiate apoptotic cascades [6]. This paper also described the activation of the mitochondrial intrinsic apoptotic pathway, as evidenced by decreased mitochondrial membrane potential, decreased cytochrome *c* content in the mitochondrial membrane and amplified caspase-9 enzymatic activity in DNR-treated H9c2 cells.

Although the precise molecular mechanisms by which anthracyclines promote mitochondrial apoptosis are not yet fully understood, the available information indicates that the ERKs signal transduction pathway plays a pivotal role in the process [9-11, 40, 41]. Extracellular signal-regulated kinases (ERKs), which are activated by DNA damaging agents, are responsible for the anthracycline-induced *p*53 activation observed in H9c2 cells [11]. The tumor suppressor *p*53 not only promotes mitochondrial dysfunction and cytochrome *c* release but also modulates the expression of the BCL-2 family proteins, thereby activating the mitochondrial apoptotic pathway [6, 11, 40]. *p*53 increases the abundance of Bcl-2 but decreases Bax, which results in an improved Bax/Bcl-2 ratio that directs cardiomyocytes toward apoptotic death [42]. The ratio of Bax to Bcl-2 protein may determine whether cells will die via apoptosis or be protected from it. The pro-apoptotic Bax promotes mitochondrial apoptosis by exacerbating mitochondrial destabilization and cytochrome *c* release, whereas the anti-apoptotic Bcl-2 antagonizes Bax [28, 43]. In the present study, we demonstrated that DNR induced apoptosis in H9c2 cells, down-regulated the expression of Bcl-2 and

increased the expression of ERKs, *p*53 and Bax. In contrast, SF sharply decreased ERK and *p*53 activation and the Bax/Bcl-2 ratio and suppressed the pro-apoptotic function of DNR. As a consequence of the reduction in apoptosis, SF effectively inhibited the DNR-induced mitochondrial apoptotic pathway, as characterized by the restoration of the mitochondrial membrane potential and cytochrome *c* content and by the decreased caspase-9 activity.

We further demonstrated that SF's ability to protect against DNR-induced cardiomyocyte apoptosis may be attributed at least partially to its ability to inhibit the ERKs signaling pathway. This idea is supported by the findings of this study, as follows: i) the SF-induced inactivation of the ERKs pathway occurred prior to the restoration of the BCL family proteins, which closely paralleled the inhibition of apoptosis; ii) similar to the cardio-protective effect of SF, the pretreatment of the H9c2 cells with AZD6244, a specific inhibitor of ERKs phosphorylation, attenuated DNR-induced growth inhibition, resulting in increased cell viability and decreased numbers of apoptotic cells; and iii) the combined use of AZD6244 and SF did not cause a significant change in cell viability or in the percentage of apoptosis compared with SF treatment alone. Each of these results was indicative of a functional link between ERKs inhibition and the anti-apoptotic efficacy of SF.

In addition, it deserves to be noted that daunorubicin is simply a model anthracycline drug. Because the cardiotoxicity shows similar features within the group, the results could be translatable to other more commonly used drugs from this class, such as doxorubicin. In addition, some limitations may impact the underlying molecular mechanisms. A major limitation of this study is that the H9c2 cell line is phenotypically different from the cardiac myocytes, though they do present several similar properties: the H9c2 cells proliferate in vitro, whereas cardiac myocytes do not proliferate [44-47]. Another limitation is the fact that most of anthracycline cardiotoxicity clinically develops on a time span of months or years, whereas experiments in cultured cells are naturally short-term (in our study, 24 h). Because the H9c2 cell model used in this study is a rough simulation of anthracycline cardiotoxicity, our results and conclusion should be acceptable as hypothesis-generating rather than definitive [48, 49]. Further exploration in primary cardiomyocytes and experimental animals is required.

In conclusion, the present study demonstrated the protective role of sodium ferulate against DNR-induced cardiotoxicity in H9c2 cells. This protective role most likely results from the inhibition of mitochondrial apoptosis via the ERKs signaling pathway. These findings may be indicative of the potential adjuvant application of SF in combination with anthracyclines to mitigate the latter's cardiotoxicity.

Acknowledgements

This research was supported by the National Natural Science Foundation of China (NSFC 31171104 and 81400236), the Doctor Startup Foundation (2010bs007) and the Key Program of Scientific Research (09ZD010) of Fujian Medical University.

Disclosure Statement

The authors declare no potential conflicts of interest.

References

1 Piekarski M, Jelinska A: Anthracyclines still prove effective in anticancer therapy. Mini Rev Med Chem 2013;13:627-634.
2 Lotrionte M, Biondi-Zoccai G, Abbate A, Lanzetta G, D'Ascenzo F, Malavasi V, Peruzzi M, Frati G, Palazzoni G: Review and meta-analysis of incidence and clinical predictors of anthracycline cardiotoxicity. Am J Cardiol 2013;112:1980-1984.

3 Sterba M, Popelova O, Vavrova A, Jirkovsky E, Kovarikova P, Gersl V, Simunek T: Oxidative stress, redox signaling, and metal chelation in anthracycline cardiotoxicity and pharmacological cardioprotection. Antioxid Redox Signal 2013;18:899-929.
4 Sheppard RJ, Berger J, Sebag IA: Cardiotoxicity of cancer therapeutics: Current issues in screening, prevention, and therapy. Front Pharmacol 2013;4:19.
5 Vejpongsa P, Yeh ET: Prevention of anthracycline-induced cardiotoxicity: Challenges and opportunities. J Am Coll Cardiol 2014;64:938-945.
6 Montaigne D, Hurt C, Neviere R: Mitochondria death/survival signaling pathways in cardiotoxicity induced by anthracyclines and anticancer-targeted therapies. Biochem Res Int 2012;2012:951539.
7 Shi J, Abdelwahid E, Wei L: Apoptosis in anthracycline cardiomyopathy. Curr Pediatr Rev 2011;7:329-336.
8 Zhang YW, Shi J, Li YJ, Wei L: Cardiomyocyte death in doxorubicin-induced cardiotoxicity. Arch Immunol Ther Exp (Warsz) 2009;57:435-445.
9 Park EJ, Kwon HK, Choi YM, Shin HJ, Choi S: Doxorubicin induces cytotoxicity through upregulation of perk-dependent atf3. PLoS One 2012;7:e44990.
10 Gharanei M, Hussain A, Janneh O, Maddock HL: Doxorubicin induced myocardial injury is exacerbated following ischaemic stress via opening of the mitochondrial permeability transition pore. Toxicol Appl Pharmacol 2013;268:149-156.
11 Liu J, Mao W, Ding B, Liang CS: Erks/p53 signal transduction pathway is involved in doxorubicin-induced apoptosis in h9c2 cells and cardiomyocytes. Am J Physiol Heart Circ Physiol 2008;295:H1956-1965.
12 Lin MC, Yin MC: Preventive effects of ellagic acid against doxorubicin-induced cardio-toxicity in mice. Cardiovasc Toxicol 2013;13:185-193.
13 Chen YL, Loh SH, Chen JJ, Tsai CS: Urotensin ii prevents cardiomyocyte apoptosis induced by doxorubicin via akt and erk. Eur J Pharmacol 2012;680:88-94.
14 Lu GH, Chan K, Leung K, Chan CL, Zhao ZZ, Jiang ZH: Assay of free ferulic acid and total ferulic acid for quality assessment of angelica sinensis. J Chromatogr A 2005;1068:209-219.
15 Ji SG, Chai YF, Wu YT, Yin XP, Liang DS, Xu ZX, Li X: Determination of ferulic acid in angelica sinensis and chuanxiong by capillary zone electrophoresis. Biomed Chromatogr 1999;13:333-334.
16 Kesh SB, Sikder K, Manna K, Das DK, Khan A, Das N, Dey S: Promising role of ferulic acid, atorvastatin and their combination in ameliorating high fat diet-induced stress in mice. Life Sci 2013;92:938-949.
17 Badawy D, El-Bassossy HM, Fahmy A, Azhar A: Aldose reductase inhibitors zopolrestat and ferulic acid alleviate hypertension associated with diabetes: Effect on vascular reactivity. Can J Physiol Pharmacol 2013;91:101-107.
18 Roy S, Metya SK, Rahaman N, Sannigrahi S, Ahmed F: Ferulic acid in the treatment of post-diabetes testicular damage: Relevance to the down regulation of apoptosis correlates with antioxidant status via modulation of tgf-beta1, il-1beta and akt signalling. Cell Biochem Funct 2014;32:115-124.
19 Alam MA, Sernia C, Brown L: Ferulic acid improves cardiovascular and kidney structure and function in hypertensive rats. J Cardiovasc Pharmacol 2013;61:240-249.
20 Koh PO: Ferulic acid prevents cerebral ischemic injury-induced reduction of hippocalcin expression. Synapse 2013;67:390-398.
21 Zhang J, Chen J, Yang J, Xu C, Ding J, Yang J, Guo Q, Hu Q, Jiang H: Sodium ferulate inhibits neointimal hyperplasia in rat balloon injury model. PLoS One 2014;9:e87561.
22 Wu ZJ, Yu J, Fang QJ, Lian JB, Wang RX, He RL, Lin MJ: Sodium ferulate protects against daunorubicin-induced cardiotoxicity by inhibition of mitochondrial apoptosis in juvenile rats. J Cardiovasc Pharmacol 2014;63:360-368.
23 Roy S, Metya SK, Sannigrahi S, Rahaman N, Ahmed F: Treatment with ferulic acid to rats with streptozotocin-induced diabetes: Effects on oxidative stress, pro-inflammatory cytokines, and apoptosis in the pancreatic beta cell. Endocrine 2013;44:369-379.
24 Huang X, Qin F, Zhang HM, Xiao HB, Wang LX, Zhang XY, Ren P: Cardioprotection by guanxin ii in rats with acute myocardial infarction is related to its three compounds. J Ethnopharmacol 2009;121:268-273.
25 Chen HP, Liao ZP, Huang QR, He M: Sodium ferulate attenuates anoxia/reoxygenation-induced calcium overload in neonatal rat cardiomyocytes by no/cgmp/pkg pathway. Eur J Pharmacol 2009;603:86-92.
26 Kim HY, Lee SM: Ferulic acid attenuates ischemia/reperfusion-induced hepatocyte apoptosis via

inhibition of jnk activation. Eur J Pharm Sci 2012;45:708-715.
27 Yang F, Zhou BR, Zhang P, Zhao YF, Chen J, Liang Y: Binding of ferulic acid to cytochrome c enhances stability of the protein at physiological ph and inhibits cytochrome c-induced apoptosis. Chem Biol Interact 2007;170:231-243.
28 Martinou JC, Youle RJ: Mitochondria in apoptosis: Bcl-2 family members and mitochondrial dynamics. Dev Cell 2011;21:92-101.
29 Ma ZC, Hong Q, Wang YG, Tan HL, Xiao CR, Liang QD, Zhang BL, Gao Y: Ferulic acid protects human umbilical vein endothelial cells from radiation induced oxidative stress by phosphatidylinositol 3-kinase and extracellular signal-regulated kinase pathways. Biol Pharm Bull 2010;33:29-34.
30 Guo R, Wu K, Chen J, Mo L, Hua X, Zheng D, Chen P, Chen G, Xu W, Feng J: Exogenous hydrogen sulfide protects against doxorubicin-induced inflammation and cytotoxicity by inhibiting p38mapk/nfkappab pathway in h9c2 cardiac cells. Cell Physiol Biochem 2013;32:1668-1680.
31 Inacio JD, Canto-Cavalheiro MM, Menna-Barreto RF, Almeida-Amaral EE: Mitochondrial damage contribute to epigallocatechin-3-gallate induced death in leishmania amazonensis. Exp Parasitol 2012;132:151-155.
32 Sagarad SV, Thakur BS, Reddy SS, Balasubramanya K, Joshi RM, Kerure SB: Elevated cardiac troponin (ctni) levels correlate with the clinical and echocardiographic evidences of severe myocarditis in scorpion sting envenomation. J Clin Diagn Res 2012;6:1369-1371.
33 Ewer MS, Ewer SM: Troponin i provides insight into cardiotoxicity and the anthracycline-trastuzumab interaction. J Clin Oncol 2010;28:3901-3904.
34 Christenson ES, James T, Agrawal V, Park BH: Use of biomarkers for the assessment of chemotherapy-induced cardiac toxicity. Clin Biochem 2014
35 Cai C, Lothstein L, Morrison RR, Hofmann PA: Protection from doxorubicin-induced cardiomyopathy using the modified anthracycline n-benzyladriamycin-14-valerate (ad 198). J Pharmacol Exp Ther 2010;335:223-230.
36 Konorev EA, Vanamala S, Kalyanaraman B: Differences in doxorubicin-induced apoptotic signaling in adult and immature cardiomyocytes. Free Radic Biol Med 2008;45:1723-1728.
37 Mordente A, Meucci E, Silvestrini A, Martorana GE, Giardina B: Anthracyclines and mitochondria. Adv Exp Med Biol 2012;942:385-419.
38 Menna P, Salvatorelli E, Minotti G: Anthracycline degradation in cardiomyocytes: A journey to oxidative survival. Chem Res Toxicol 2010;23:6-10.
39 Sardao VA, Oliveira PJ, Holy J, Oliveira CR, Wallace KB: Doxorubicin-induced mitochondrial dysfunction is secondary to nuclear p53 activation in h9c2 cardiomyoblasts. Cancer Chemother Pharmacol 2009;64:811-827.
40 Matissek KJ, Mossalam M, Okal A, Lim CS: The DNA binding domain of p53 is sufficient to trigger a potent apoptotic response at the mitochondria. Mol Pharm 2013;10:3592-3602.
41 Yee KS, Vousden KH: Contribution of membrane localization to the apoptotic activity of puma. Apoptosis 2008;13:87-95.
42 Comelli M, Domenis R, Bisetto E, Contin M, Marchini M, Ortolani F, Tomasetig L, Mavelli I: Cardiac differentiation promotes mitochondria development and ameliorates oxidative capacity in h9c2 cardiomyoblasts. Mitochondrion 2011;11:315-326.
43 Branco AF, Pereira SL, Moreira AC, Holy J, Sardao VA, Oliveira PJ: Isoproterenol cytotoxicity is dependent on the differentiation state of the cardiomyoblast h9c2 cell line. Cardiovasc Toxicol 2011;11:191-203.
44 Menard C, Pupier S, Mornet D, Kitzmann M, Nargeot J, Lory P: Modulation of l-type calcium channel expression during retinoic acid-induced differentiation of h9c2 cardiac cells. J Biol Chem 1999;274:29063-29070.
45 Sardao VA, Oliveira PJ, Holy J, Oliveira CR, Wallace KB: Morphological alterations induced by doxorubicin on h9c2 myoblasts: Nuclear, mitochondrial, and cytoskeletal targets. Cell Biol Toxicol 2009;25:227-243.
46 Branco AF, Sampaio SF, Moreira AC, Holy J, Wallace KB, Baldeiras I, Oliveira PJ, Sardao VA: Differentiation-dependent doxorubicin toxicity on h9c2 cardiomyoblasts. Cardiovasc Toxicol 2012;12:326-340.
47 Pereira SL, Ramalho-Santos J, Branco AF, Sardao VA, Oliveira PJ, Carvalho RA: Metabolic remodeling during h9c2 myoblast differentiation: Relevance for in vitro toxicity studies Cardiovasc Toxicol 2011;11:180-190.